PAN

Opto-Electronics Review

journal homepage: https://journals.pan.pl/opelre

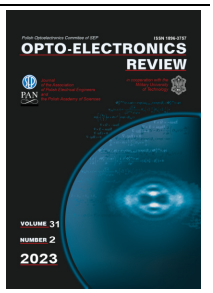

Design and performance evaluation of vehicular visible light communication system under different weather conditions and system parameters

Eslam S. El-Mokadem[1], Nagwan I. Tawfik[1], Moustafa H. Aly[2*], Walid S. El-Deeb[3]

[1]Department of Electronics and Communications Engineering, Higher Technological Institute, 10th of Ramadan City, Egypt
[2]Arab Academy for Science, Technology and Maritime Transport, 1029 Alexandria, Egypt
[3]Department of Electronics and Communications Engineering, Zagazig University, 44519 Zagazig, Egypt

Article info

Article history:
Received 05 Jan. 2023
Received in revised form 24 Feb 2023
Accepted 24 Feb 2023
Available on-line 11 Apr 2023

Keywords:
Visible light communication; beam divergence; bit error rate; vehicular communication; laser diode.
.

Abstract

Vehicular visible light communication is an emerging technology that allows wireless communication between vehicles or between vehicles and infrastructure. In this paper, a vehicular visible light communication system is designed using a non-return to zero on-off keying modulation scheme under the effect of different weather conditions such as clear, haze, and fog. The first model is a light emitting diode-based system and the second is a laser diode-based system. For both models, the influence of system parameters such as beam divergence, transceiver aperture diameters, and receiver responsivity is studied. The impact of the use of the trans-impedance amplifier is also investigated for both models. It was concluded that in the presence of the amplifier, output power of the light emitting diode and laser diode model are increased by 98.46 μW and 0.4719 W, respectively. The performance of the two proposed models is evaluated through bit error rate, quality factor, eye diagram, and output power to have some insightful results about the quality of service for the two proposed models. Under a specific weather condition, the performance of the system would be critical and other techniques should be applied. The maximum achievable link distance for the laser-based and light-emitting diode-based systems is 190 m at a data rate of 25 Gbps and 80 m at a data rate of 60 kbps, respectively, under the same system parameters and weather conditions. The obtained results provide a full idea about the availability of constructing our proposed model in a practical environment, showing a higher performance of the laser diode-based model than that of the light emitting diode-based model.

1. Introduction

Optical wireless communication (OWC) is one of the novel communication technologies that utilize the infrared (IR) band, visible light (VL) band, or ultraviolet (UV) band. One of the promising applications for the future technological world to implement Internet of Things (IoT) in the future fifth-generation networks is vehicle-to-vehicle (V2V) communications. The increasing demand for IoT, mobile internet, and the limited radio frequency spectrum imposes several challenging requirements for 5G wireless communications, such as high throughput, massive connectivity, high reliability, and low latency [1, 2]. It is imperative to design new communication technologies to overcome the drawbacks of radio frequency (RF) communication systems. Visible light communication (VLC) technology is considered an alternative technology that can provide more advantages over RF as light can be used as the transmission carrier which can provide both illumination and communication simultaneously, its license is free, more secure, free from electromagnetic interference and can provide a huge bandwidth. Moreover, VLC is a free space optic (FSO) technology where a data rate of 10 Gbps and beyond can be obtained. RF technology supports a data rate lower than that obtained with VLC

*Corresponding author at: mosaly@aast.edu

https://doi.org/10.24425/opelre.2023.145580
1896-3757/ Association of Polish Electrical Engineers (SEP) and Polish Academic of Sciences (PAS). Published by PAS

communication systems. VLC systems can be used in many applications in different environments such as hospitals, underwater, and vehicular systems [3]. Vehicular communication systems depend mainly on the use of high beam or low beam headlamps as a light emitting diode (LED) which can be used as an optical transmitter. It has many advantages such as low cost, high efficiency, ease of handling, and low power consumption. At the receiver side, an avalanche photodiode (APD) or a positive intrinsic negative (PIN) photodiode can be used [4]. This technology enables drivers to exchange information, including congested traffic areas, the distance between vehicles, etc. The modulation process is performed at the intensity of the light waves. This type of modulation is called intensity modulation (IM). At the receiving end, the detection of the original signal is performed by the photodiode receiver by a scheme called a direct detection (DD) technique. Different modulation schemes can be used in VLC systems such as on-off keying (OOK), pulse code modulation (PCM), and pulse amplitude modulation (PAM) [5]. The most widely used modulation scheme in OWC systems is OOK which is easy and simple to implement.

Recently, numerous advanced research works have been made on vehicular VLC systems. For example, in Ref. 6, the authors investigate the performance of the VLC system under the effect of background noise. A LED has been used as the optical transmitter and the PIN photodiode has been used as the optical receiver. A data rate of 20 Kbps has been obtained using a return-to-zero (RZ-OOK) modulation scheme. A link distance of 20 m has been obtained for that work. In Ref. 7, the performance of VLC system has been studied using the Optisystem simulation tool. A white LED has been used as a transmitter. Non-return-to-zero (NRZ-OOK) modulation scheme has been used. For a data rate of 2G bps and a link distance of 3 m, the obtained maximum Q-factor was 5.76 which is not suitable for applying this system in a practical environment. In Ref. 8, the authors propose an experimental demonstration of a V2V OWC system. A data rate of 100 Mbps is obtained for a link distance of 2 m and a data rate of 14 Mbps is obtained for a link distance of 15 m. In Ref. 9, the authors investigate the performance of VLC system with orthogonal frequency division multiplexing (OFDM)-modulated white LED with the help of an Optisystem simulation tool. Performance evaluation for the system has been investigated only for specific weather conditions and the effect of other environmental conditions has been neglected. A 10 Gbps data rate can be supported by the proposed system up to a link distance of 2 with an accepted bit error rate (BER). In Ref. 10, the authors investigate the performance of a vehicle-to-everything (V2X) communication system using a direct sequence optical code division multiple access (DS-OCDMA) technique.

But, in the previously mentioned works, the authors neglect the effect of different weather conditions and the effect of system parameters on the performance of the system. Ref. 11 investigates the effect of different weather conditions on the performance of a free space optical communication system under real-world atmospheric conditions. But the effects of all system parameters such as beam divergence, transceiver aperture diameters, receiver responsivity, and quantum efficiency have not been investigated. Weather conditions play an important role in degrading the performance of such systems. Some of the main sources of atmospheric attenuation are due to fog, haze, rain, or dust. Regarding the size of the particles, there are three different ranges that can be taken under consideration. The main parameter required for the calculation of atmospheric attenuation is visibility. According to the visibility of the link, the size of the particles in the atmosphere, and the type of scattering, the attenuation can be predicted.

This paper concentrates on designing and evaluating the performance of a V2V VLC system under the effect of different weather conditions and system parameters for different data rates and link distances. Two proposed models have been applied with different optical transmitters. The first one depends on the use of a LED that represents the high-beam headlamp of the system. The second one uses a laser diode (LD) as the optical transmitter. A practically measured APD has been used as the optical receiver for both models. An NRZ-OOK modulation scheme has been used. The two proposed models are evaluated by calculating BER, quality factor (Q-factor), eye diagram, and output power to have some insightful results about the quality of service (QoS) for the two proposed models. The analysis showed that vehicular visible light communication (VVLC) system-based LD is better than VVLC system-based LED under the effect of different weather conditions for the same modulation scheme and system parameters.

This paper is prepared as follows: section 2 describes the mathematical analysis for the VVLC system model. Then the first proposed model based on LED has been studied followed by studying the effect of system parameters and the impact of link distance under the effect of different weather conditions. Section 3 illustrates the second proposed model of the VVLC system based on LD followed by studying the effect of system parameters and the impact of link distance under different weather conditions. Section 4 demonstrates comparisons between the obtained simulation results and the mathematical results for different weather conditions for both proposed models. Finally, the concluding remarks are provided in section 5 of this paper.

2. Mathematical analysis for the proposed vehicular visible light communication models

We consider a LED-based VVLC system in the first proposed model. In the second model, an LD is used as the optical transmitter. One of the high-beam or low-beam headlamps of the source vehicle serves as an optical transmitter. The destination vehicle is equipped with an APD as an optical receiver. The APD is mounted at the same height as the source headlamps and looks backward as illustrated in Fig. 1.

The basic block diagram for the proposed VVLC system using the NRZ-OOK modulation scheme is illustrated in Fig. 2.

The transmitter is used for modulating the message signal onto the optical carrier for propagation in a free space channel. It contains three main components: modulator, optical source such as LED or LD, and transmitting antenna or telescope. The transmitter consists of a pseudo-random bit sequence generator (PRBSG), a pulse generator and an LED or an LD which represents the

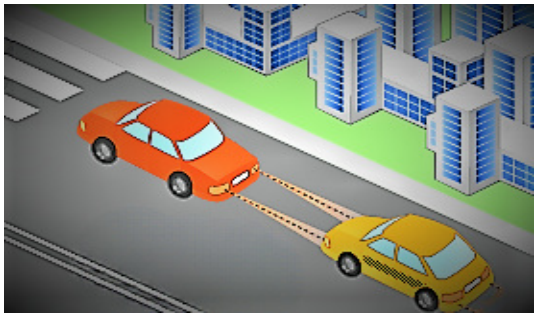

Fig. 1. Scenario for the V2V-VLC system

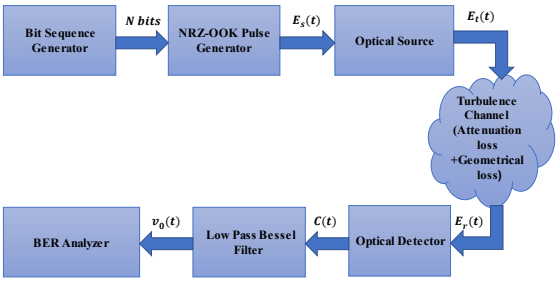

Fig. 2. Block diagram for the proposed VVLC system.

high beam headlamp of the vehicle. The PRBSG is used to generate the bit stream. This type of generators can generate the stream of bits randomly. An NRZ pulse generator is then used to convert the stream of bits into an electrical signal. An NRZ modulation scheme is used in our proposed model, and in VLC systems generally, because it has more energy than the RZ modulation scheme, easy to implement and is suitable for use in VVLC systems. The electrical signal is then passed through the optical source which produces an optical power of 1 W in our proposed models. The field amplitude is projected along the horizontal $\bar{x}$ and vertical $\bar{y}$ axes and can be described as [12]

$$\overline{E_x} = A_x \exp(j(wt - k_z)\bar{x}, \tag{1}$$

$$\overline{E_y} = A_y \exp(j(wt - k_{z+\varphi})\bar{y}, \tag{2}$$

where A_x and A_y represent the electric field amplitudes on the $\bar{x}$ and $\bar{y}$ directions, w – the angular frequency, k_z – wave vector in z direction and φ is the phase difference between the two electric field components.

Assuming a linearly polarized signal along the $\bar{x}$ axis only, the transmitted signal will be given by

$$\overline{E_s(t)} = \sqrt{\frac{P_T}{2}} \exp j[wt + \varphi_s(t)], \tag{3}$$

where P_T is the transmitted power. The transmitted optical field at the output of the transmitter can be expressed as

$$\overline{E_t(t)} = \sqrt{\frac{P_T}{2}} \exp[wt + \varphi_t(t)]\ m(t)\bar{x}, \tag{4}$$

$$m(t) = \sum_{k=-\infty}^{\infty} b_k\ rect_T(t - kT), \tag{5}$$

where b_k is the transmitted bit and equals 0 or 1, T is the symbol period and $m(t)$ is the rectangular function.

$$\text{rect}_T(t) = \begin{cases} 1; & t \in (0,\pi) \\ 0; & \text{elsewhere.} \end{cases} \tag{6}$$

After passing through the atmospheric channel, the received optical signal from the channel is given by

$$\overline{E_r(t)} = \sqrt{\frac{P_r}{2}} \exp[j(wt + \varphi_r(t))]\ m(t), \tag{7}$$

where P_r is the received power and φ_r is the phase noise of the receiver.

The received optical power can be expressed as

$$P_R = P_T \frac{d_R^2}{(d_T + \theta L)^2} e^{-\alpha L}, \tag{8}$$

where d_R is the receiver aperture diameter, d_T is the transmitter aperture diameter, θ is the beam divergence, L is the link distance, and α is the atmospheric attenuation. The photodetector detects the optical received signal $E_r(t)$ and converts it into an electrical signal.

The output of the photodiode can be expressed as

$$C(t) = R\ |E_r(t)|\ m(t) + n(t), \tag{9}$$

where R is the responsivity of the receiver and $n(t)$ represents the system noise term which can be considered as the thermal noise and the background noise.

The output of the photodiode can be expressed as

$$C(t) = R \left| \sqrt{\frac{P_r}{2}} \right|^2 m(t) + n(t). \tag{10}$$

Assuming an undistorted signal, the output of the receiver can be given by

$$C(t) = R \frac{P_R}{2}\ m(t) + n(t). \tag{11}$$

The output of the photodiode is then passed through a low pass Bessel filter (LPF) with a transfer function given by [12]

$$H(s) = I \frac{d_0}{B_N(s)}, \tag{12}$$

where I is the insertion loss parameter, N is the parameter order, d_0 is the normalizing constant, and $B_N(s)$ is the nth order Bessel polynomial

$$d_0 = \frac{(2N)!}{2^N \cdot N!}, \tag{13}$$

$$B_N(s) = \sum_{k=0}^{N} d_k\ s^k, \tag{14}$$

$$d_k = \frac{(2N-k)!}{2^{N-k}\ k!\ (N-k)!}, \tag{15}$$

$$S = j\left(\frac{f \cdot \omega_b}{f_c}\right), \tag{16}$$

where f_c is the cutoff frequency defined by the parameter frequency and ω_b is the normalized 3 dB bandwidth.
The normalized 3 dB bandwidth can be calculated as shown in Ref. 12. Then, the output of the LPF can be expressed as [12]

$$\omega_b \approx \sqrt{(2N-1)\cdot \ln 2} \tag{17}$$

$$v_0(t) = \frac{1}{T}\int_0^T C(t)\cdot h(t) = \begin{cases} \frac{-RP_R}{2} + n_{LPF}; & m(t) = 0 \\ \frac{RP_R}{2} + n_{LPF}; & m(t) = 1. \end{cases} \tag{18}$$

where $h(t)$ is the impulse response of the LPF, T is the symbol period and n_{LPF} is the white Gaussian noise that can be given by

$$n_{LF} \approx \left[0, \frac{\sigma_n^2}{2}\right], \tag{19}$$

where σ_n^2 is the noise variance.

The range of the signal $v_0(t)$ is A_{on} and A_{off} where $A_{on} = \frac{RP_R}{2}$ and $A_{off} = \frac{-RP_R}{2}$ for the transmission of 1 and 0, respectively. In this case the threshold level is at zero level.

The probability density function (PDF) can be given by

$$\text{PDF} = \frac{1}{\sqrt{2\pi\sigma_n^2}}\int_0^{\infty} \exp\left(-\frac{(v-m)^2}{2\sigma_n^2}\right) dv. \tag{20}$$

The PDF can be used for determining the probability of error in the proposed system.

For logic 1 pulses, all of amplitude v will have a mean and variance of A_{on} and σ_{on}^2. So, the probability of error is equal to the probability that the noise will exceed the threshold voltage (v_{th}), which is mistaken for a 0 pulses. It is given by

$$P_1(v_{th}) = \frac{1}{\sqrt{2\pi\sigma_{on}^2}}\int_{-\infty}^{v_{th}} \exp\left(-\frac{(A_{on}-v)^2}{2\sigma_n^2}\right) dv. \tag{21}$$

For logic 0 pulses with a mean and variance of A_{off} and σ_{off}^2, the probability of error in the presence of 0 bit is given by

$$P_0(v_{th}) = \frac{1}{\sqrt{2\pi\sigma_{off}^2}}\int_{v_{th}}^{\infty} \exp\left(-\frac{\left(v-A_{off}\right)^2}{2\sigma_n^2}\right) dv, \tag{22}$$

where $P_1(v_{th})$ and $P_0(v_{th})$ indicate the error probability in the presence of 1 bit and 0 bit, respectively.

The total error probability can be given by

$$F(V) = \frac{1}{2}P_1(v_{th}) + \frac{1}{2}P_0(v_{th}). \tag{23}$$

Assuming that the probability of error in the presence of 0 and 1 pulses are equally likely, thus, the BER can be given by

$$\text{BER} = \frac{1}{\sqrt{2\pi}}\left(\frac{\exp\left(Q^2/2\right)}{Q}\right), \tag{24}$$

where Q represents the quality of the signal-to-noise ratio (SNR) in the eye diagram and is given by

$$Q = \frac{v_{th} - A_{off}}{\sigma_{off}} = \frac{A_{on} - v_{th}}{\sigma_{on}} = \frac{A_{on} - A_{off}}{\sigma_{on} + \sigma_{off}}. \tag{25}$$

The average BER can be given as

$$\text{BER} = \frac{1}{\sqrt{2\pi\sigma_n^2}}\int_0^{v_{th}}\int_0^{\infty} \exp\left(-\frac{\left(v-\frac{RP_R}{2}\right)^2}{\sigma_n^2}\right) P(I)\,dv\,dI. \tag{26}$$

After performing some mathematical expression transformation, the BER can be calculated as

$$\text{BER} = \frac{1}{2}\left(\text{erfc}\left(\frac{|A_{on} - v_{th}|}{\sigma_{on}}\right) + \text{erfc}\left(\frac{|v_{th} - A_{off}|}{\sigma_{off}}\right)\right), \tag{27}$$

$$\text{BER} = \frac{1}{2}\text{erfc}\left(\frac{RP_R}{2\sigma_n}\right), \tag{28}$$

where σ_n is the standard deviation and erfc(.) denotes the complementary error function.

The closed form approximation of BER for NRZ-OOK can be given by

$$\text{BER} = \frac{1}{2}\text{erfc}\left(\frac{Q}{\sqrt{2}}\right), \tag{29}$$

where

$$Q = \frac{\sqrt{2}\,R\,P_R}{2\sigma_n}. \tag{30}$$

2.1. Proposed system model setup using light emitting diode

A high beam headlamp of a Philips Luxeon Rebel white LED type is used in the first proposed model. Table 1 illustrates the specifications of the high beam headlamp of the vehicle used in our proposed model.

Table 1.
Specifications of the LED-based high beam headlamp [13].

Parameter	Value
Type	High beam headlamp white LED
Power	1 W
Light wavelength	400–700 nm

The output optical power can be expressed as [9]

$$P = \eta \cdot h \cdot f \cdot \frac{i(t)}{q_e}, \tag{31}$$

where η is the quantum efficiency, h is Planck's constant, f is the emission frequency, $i(t)$ is the input electrical signal, and q_e is the electron charge.

The channel environment in vehicular VLC systems plays an important role in the system performance [14]. Thus, the effect of the channel parameters should be studied accurately. In our proposed system, the effect of attenuation losses and geometrical losses are taken under consideration. The attenuation losses can be called atmo-spheric losses, which indicate the loss in the transmitted signal power. This loss is produced mainly due to atmospheric turbulences [9]. In our proposed work, the effect of three different weather conditions has been investigated. Table 2 shows different weather conditions and the attenuation loss due to each weather condition [15]. Table 3 shows the parameters settings of the FSO channel.[9].

Table 2.
Attenuation loss due to different weather conditions [14].

Weather condition	Attenuation loss (dB/km)
Clear	0.4
Haze	4
Fog	21

Table 3.
Parameters settings for the wireless channel.

Parameter	Value
Link distance	80 m
The aperture diameter of the transmitter telescope	7 cm
The aperture diameter of the receiver telescope	1.5 cm
Beam divergence angle	68 mrad

On the other hand, the effect of the geometrical loss appears in the form of beam width spread between the transmitter and receiver. The beam spreads to a size which is larger than the receiver aperture diameter. The geometrical loss (GL) is given by [15]

$$\mathrm{GL}(dB) = -20\log\left[\frac{d_R}{(d_T + \theta L)}\right]. \tag{32}$$

The choice of the optical receiver should satisfy the requirements of cost, safety, and performance. There are different types of optical receivers that can be used in VLC systems such as APD and PIN diode [16–18]. In the proposed model, a practically measured APD of type (Si) Hamamatsu [S8664-1010] is used [19]. The effect of thermal noise and shot noise has been taken into account according to the parameters of the APD which is illustrated in Table 4.

Table 4.
Parameters of the APD [S8664-1010] [19].

Parameter	Value
Gain	50
Bandwidth	65 MHz
Surface dark current	10 nA
Noise figure	0.2
Responsivity	0.28 A/W
Load resistance	50 Ω

To reduce the effect of these noises on the system performance, an LPF has been used. The total noise variance is given by [20]

$$\sigma_{total}^2 = \sigma_{shot\ noise}^2 + \sigma_{thermal\ noise}^2. \tag{33}$$

The shot noise is given by [20]

$$\sigma_{shot\ noise}^2 = 2q_e G^2 F(I_{inc})B, \tag{34}$$

where F is the excess noise, q_e is the electron charge, G is the photodiode gain, B is the photodiode bandwidth. The photocurrent produced, I_{inc}, due to the received optical power is given by

$$I_{inc} = GA_r \int_{\lambda_1}^{\lambda_2} P_{inc}(\lambda)R(\lambda)T_0(\lambda)d\lambda, \tag{35}$$

where λ_1 and λ_2 are the visible light wavelengths, $R(\lambda)$ is the responsivity of the APD, A_r is the effective area of the receiver, $T_0(\lambda)$ is the transmittance of the bandpass optical filter. The shot noise distribution in our proposed model is Gaussian. The thermal noise is given by

$$\sigma_{thermal}^2 = 4\left(\frac{k_B T_k}{R_l}\right)F_n B, \tag{36}$$

where k_B is the Boltzmann constant, R_l is the load resistance, T_k is the absolute temperature, B is the photodiode bandwidth and F_n is the noise figure.

An LPF with 4th order has been used in the proposed model.

2.2. *Effect of the transimpedance amplifier in the light emitting diode-based model.*

Figures 3 and 4 illustrate the Q-factor and the eye diagram obtained for the proposed model. In digital communication systems, the eye diagram indicates the quality of the signal. The Q-factor can be used for representing the quality of the SNR in the eye of a digital signal. The 'eye' being the human eye-shaped pattern on an oscilloscope that shows the transmission system performance.

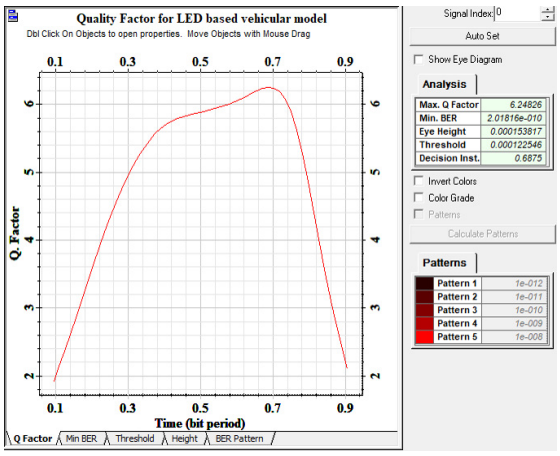

Fig. 3. Q-factor for the LOS model using LED with a link distance of 80 m and a data rate of 60 kbps.

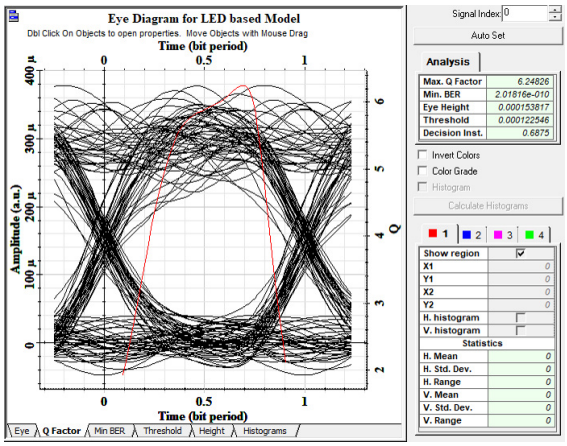

Fig. 4. Eye diagram for the LOS model using LED with a link distance of 80 m and a data rate of 60 kbps.

For better performance of the system and for enhancing the output electrical power at the receiving end, a trans-impedance amplifier (TIA) can be used for increasing the output electrical power. The TIA is used to convert the output current of the APD into an electrical voltage and also for increasing the output electrical power at the receiving end. Tables 5 and 6 show the power calculations for the line of sight (LOS) model without and with TIA, respectively.

Table 5.
Power calculations of the proposed model without using TIA.

	Signal power		Noise power	
	Watt	**dBm**	**Watt**	**dBm**
The output power of high beam headlamp	1.393	31.44	0	−100
The output power of the channel	$10.2 \cdot 10^{-6}$	−19.8	0	−100
The output power of APD	$64.7 \cdot 10^{-9}$	−41.8	$16 \cdot 10^{-9}$	−47.7
The output power of LPF	$39.4 \cdot 10^{-9}$	−44	$343.6 \cdot 10^{-12}$	−64

Table 6.
Power calculations of the proposed model using TIA.

	Signal power		Noise power	
	Watt	**dBm**	**Watt**	**dBm**
The output power of high beam headlamp	1.393	31.44	0	−100
The output power of the channel	$10.2 \cdot 10^{-6}$	−19.8	0	−100
The output power of APD	$64.7 \cdot 10^{-9}$	−41.8	$16 \cdot 10^{-9}$	−47.7
The output power of TIA	$161 \cdot 10^{-6}$	−7.9	$41 \cdot 10^{-6}$	−13.79
The output power of LPF	$98.5 \cdot 10^{-6}$	−10	$859 \cdot 10^{-9}$	−30.66

From the obtained results, it is clear that the TIA has a significant effect on the output electrical power as there is an increase in the output power by 98.46 μW when compared with the model which includes no TIA. The presence of the TIA has no effect in the values of both the Q-factor and BER. The obtained values for the maximum Q-factor and the minimum BER are acceptable, as for a good signal reception, the maximum Q-factor should be higher than 6 and the minimum BER should be lower than 10^{-9}. The maximum quality factor obtained for our model is 6.248 and the minimum BER is $2.018 \cdot 10^{-10}$.

2.3. Impact of link distance under different weather conditions for the light emitting diode-based model.

Now, the system performance is evaluated according to different affecting parameters that have a significant effect on the maximum Q-factor, minimum BER, and output electrical power. Weather conditions have a significant impact on the performance of the vehicular VLC system [21, 22]. The response of the system to different weather conditions is investigated. The effect of different parameters such as link distance, data rate, receiver aperture diameter, receiver responsivity, beam divergence, and quantum efficiency on the performance of the system is discussed. Figure 5 displays the effect of link distance on the maximum Q-factor for a data rate of 60 kbps. As illustrated in Fig. 5, for distances up to ~30 m, the link distance has no effect on the value of the maximum Q-factor. The change of the weather condition does not affect the performance of the system, also. After that, as the link distance is increased, the maximum Q-factor decreases until reaching an acceptable value of 7.24 for fog weather condition at a link distance of 60 m. For clear sky and haze weather conditions, it reaches the values of 8.1 and 7.96, respectively. This system can support up to 60 m link distance with an acceptable value of the maximum Q-factor (7.24) for the worst case of the weather conditions (fog weather condition) with an attenuation loss α = 21 dB/km.

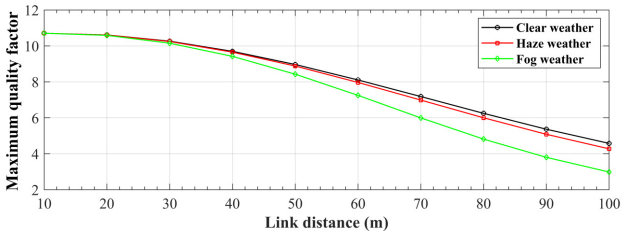

Fig. 5. Maximum Q-factor *vs.* link distance under different weather conditions.

The weather conditions have a great influence on the quality of the OWC system [23]. The received signal power is affected by different weather conditions such as rain, snow, and fog. Regarding the size of the particles, there are three different ranges that can be taken under consideration. In case of fog, tiny particles are considered. In this case, Mie-scattering is used to calculate the effect of fog [11]. This approach is sophisticated and detailed parameters are required for estimating the effect of fog. Another method [24] which is simpler and depends on the value of the visibility can be used. An empirical model for Mie-scattering is used to calculate the attenuation coefficient. The attenuation loss, α, in dB/km, is given by [11]

$$\alpha = 10 \log_e[\gamma(\lambda)] \tag{37}$$

with

$$\gamma(\lambda) = \frac{3.91}{V}\left(\frac{\lambda}{550\,\text{nm}}\right)^{-T}, \tag{38}$$

where V is the visibility range, λ is the operating wavelength, and T is the coefficient that describes the fog thickness. This coefficient can be calculated according to the Kruse model in terms of the visibility factor as [25]

$$T = \begin{cases} 1.6, & V > 50 \\ 1.3, & 6 < V < 50 \\ 0.585V^{1/3}, & V < 6\,. \end{cases} \tag{39}$$

Figures 6–8 show the effect of link distance on the value of BER for different weather conditions. It is noted that as the distance is increased, the BER is increased until it reaches $9.93 \cdot 10^{-10}$ for fog with a link distance of 70 m. For clear and haze weather conditions, the BER reaches its minimum acceptable value at a link distance of 80 m. At this distance, the BER for clear sky is $2.02 \cdot 10^{-10}$ and for haze, it reaches a value of $9.62 \cdot 10^{-10}$.

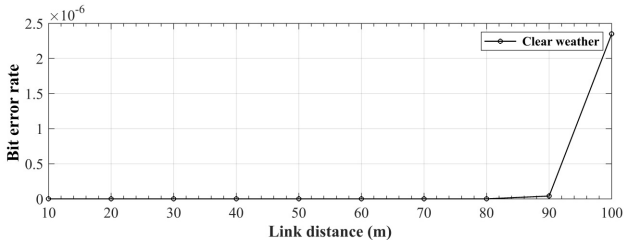

Fig. 6. BER *vs*. link distance for clear sky weather.

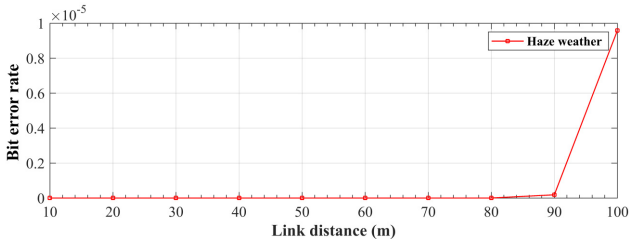

Fig. 7. BER *vs*. link distance for haze weather.

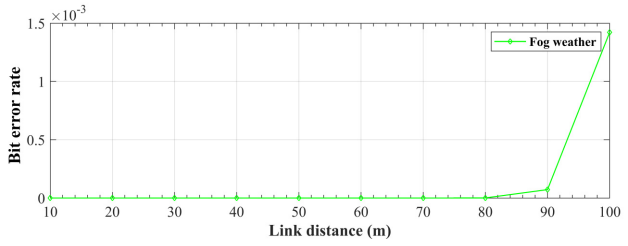

Fig. 8. BER *vs*. link distance for fog weather.

The link distance also has a strong influence on the received output power. At the receiving end, the received power intensity decreases with the square root of the link distance. Thus, the output power decreases with the link distance. Figure 9 shows the effect of link distance on the received electrical power at a data rate of 60 kbps. The output electrical power decreases exponentially with the link distance until reaching a value of −4.068 dBm at a link distance of 50 m for fog weather, where α = 21 dB/km.

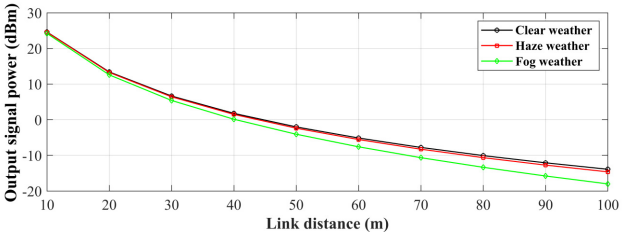

Fig. 9. Output electrical power *vs*. link distance under different weather conditions.

2.4. Performance evaluation of the first proposed model under different system parameters.

In this section, the effect of different system parameters is investigated, including receiver aperture diameter, beam divergence, receiver responsivity, and quantum efficiency. The effect of the data rate on the maximum Q-factor is also discussed. The relation between maximum Q-factor and the receiver aperture diameter, at a link distance of 80 m and a data rate of 60 kbps, is illustrated in Fig. 10. An increase in the maximum Q-factor is noticed with the increase of the receiver aperture diameter until it reaches ~7 cm. For values higher than 7 cm of the receiver aperture diameter, the value of the maximum Q-factor remains approximately constant with the increase of the receiver aperture diameter.

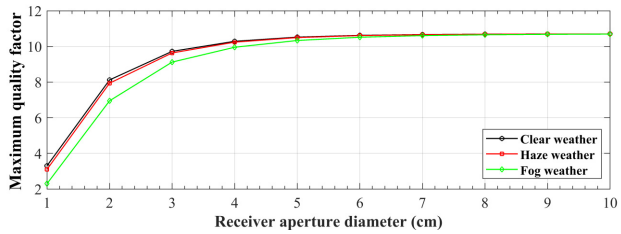

Fig. 10. Maximum Q-factor *vs*. the receiver aperture diameter under different weather conditions at a link distance of 80 m and a data rate of 60 kbps.

The ability of transmitting a very narrow optical beam is one of the main advantages of OWC systems. Diffraction occurs to the light beam while travelling from the transmitter to the receiver. This reduces the amount of light which is collected by the receiver aperture. The loss in the uncollected beam is called “beam divergence loss". The beam divergence is a measure of how fast a light beam expands far from its focus. As the beam divergence is decreased, the obtained scattering is decreased leading to a good system performance. Figure 11 shows the beam divergence between the transmitter and receiver. Figure 12 shows the relation between beam divergence and maximum Q-factor for a link distance of 80 m and a data rate of 60 kbps. This parameter describes the attenuation between the transmitter and the receiver. This loss depends on the light beam width and the diameter of the telescope at the receiving end. For the LED-based model, the small values of the beam divergence do not affect the value of the maximum Q-factor. For a beam divergence ranging from 1 to 12 mrad, the maximum Q-factor is approximately still constant and does not change with the change of the beam divergence. After a beam divergence of 12 mrad, the maximum Q-factor decreases with the increase of the beam divergence until it reaches an acceptable value of 6 at a beam divergence of 58 mrad for fog weather condition.

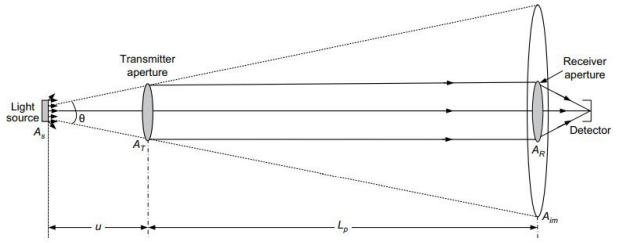

Fig. 11. Beam divergence [26].

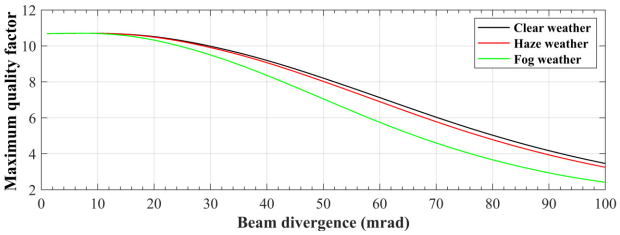

Fig. 12. Maximum Q-factor *vs*. beam divergence under different weather conditions.

The key parameter in the APD is its responsivity, which is a measure of the PD sensitivity to the input light. The responsivity of the APD is given by [22]

$$R = \frac{I_p}{P}, \tag{40}$$

where I_p is the output current of the PD and P is the incident light power. The physical structure of the APD affects the value of the responsivity. The effective area of the APD should be large enough to have the ability of collecting enough optical power. Figure 13 displays the maximum Q-factor *vs*. receiver responsivity under different weather conditions. Clearly, as the responsivity is increased, the maximum Q-factor increases significantly for small values of the receiver responsivity. For good system performance, it is better to choose a receiver responsivity higher than 0.4 A/W.

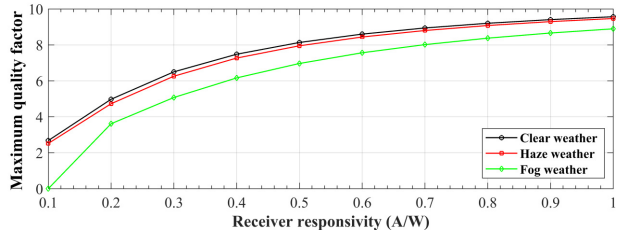

Fig. 13. Maximum Q-factor *vs*. receiver responsivity under different weather conditions.

The quantum efficiency also has strong effect on the performance of the wireless systems which depends on the use of LED as a light source. Figure 14 displays the effect of quantum efficiency on the system performance, where the Q-factor increases with the quantum efficiency. It is better to have a quantum efficiency higher than 0.8 for better performance of the system under different weather conditions. Figure 15 shows the effect of data rate on the value of the maximum Q-factor for a link distance of 80 m. The figure depicts that the best suitable values for the maximum Q-factor can be obtained at a data rate of 60 kbps. At this data rate, the corresponding maximum Q-factor is 6.24, 6, and 4.81 for clear sky, haze, and fog conditions, respectively.

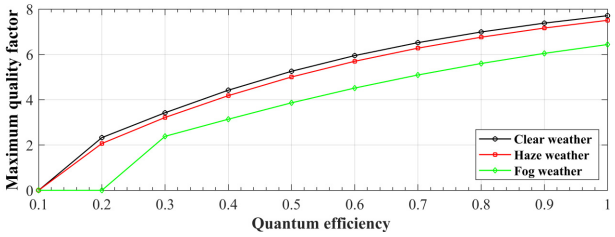

Fig. 14. Maximum Q-factor *vs*. quantum efficiency under different weather conditions.

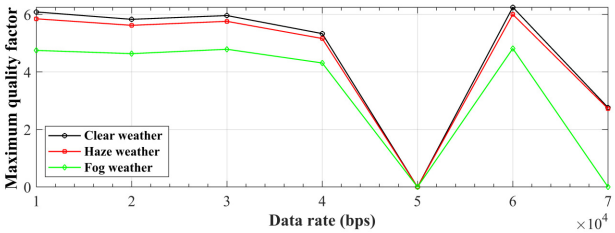

Fig. 15. Maximum Q-factor *vs*. data rate under different weather conditions.

3. Laser diode-based vehicular visible light communication (VVLC) system setup.

More attention has been paid towards the use of LD instead of the traditional LED due to its higher modulation bandwidth, higher beam convergence, and higher efficiency. The proposed system model depends on the use of LD as the optical transmitter and an APD as the optical receiver. Indium-gallium-nitride diode lasers with an output power of 1 W are used in our proposed model. The proposed system can support up to a data rate of 25 Gbps and a link distance of 190 m. This shows that this system is better than the first proposed system (the LED-based one) as it can support a higher data rate and higher link distance.

Table 7 shows the simulation parameters for the LD. This model uses the same optical receiver which was used in the first model which is a practically measured APD of type (Si) Hamamatsu [S8664-1010]. Table 8 shows the simulation parameters of the wireless channel.

Table 7.
Simulation parameters for LD [10].

Parameter	Value
Wavelength	450 nm
Power	1 W
Extinction ratio	10 dB
Linewidth	10 MHz
Initial phase	0°

Table 8.
Parameters settings for wireless channel [9].

Parameter	Value
Range	190 m
Attenuation	0.4, 4 and 21 dB/km
Transmitter aperture diameter	1 cm
Receiver aperture diameter	1.5 cm
Beam divergence	2 mrad

For systems with higher data rates, a beam divergence with a value of 2 mrad should be selected. Figure 16 displays the Q-factor for the proposed model. The obtained maximum Q-factor for the proposed model is 6.419 and the corresponding BER is $6.81 \cdot 10^{-11}$. When compared with the first model (the LED-based one), the new model (the LD-based one) is seen to outperform the first model as it has a higher Q-factor and lower BER as shown in Table 9. Figure 17 demonstrates the eye diagram for the LOS model using LD with a link distance of 190 m and a data rate of 25 Gbps.

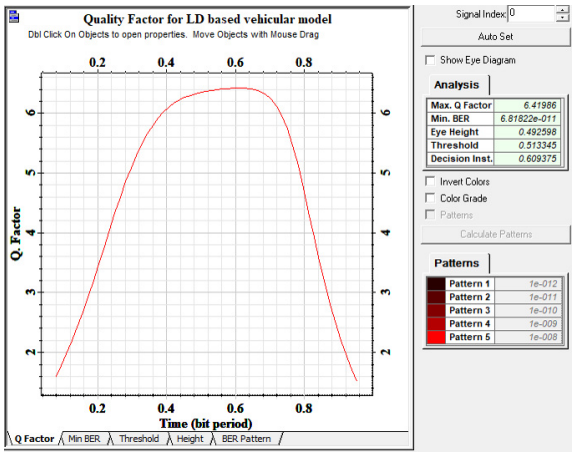

Fig. 16. Q-factor for the proposed model using LD with a 190 m link distance at 25 Gbps.

Table 9.
Comparison between the two proposed models concerning both Q-factor and BER.

	Max. Q-factor	BER	Link distance (m)	Data rate
LED-based model	6.248	$2.018 \cdot 10^{-10}$	80	60 kbps
LD-based model	6.419	$6.81 \cdot 10^{-11}$	190	25 Gbps

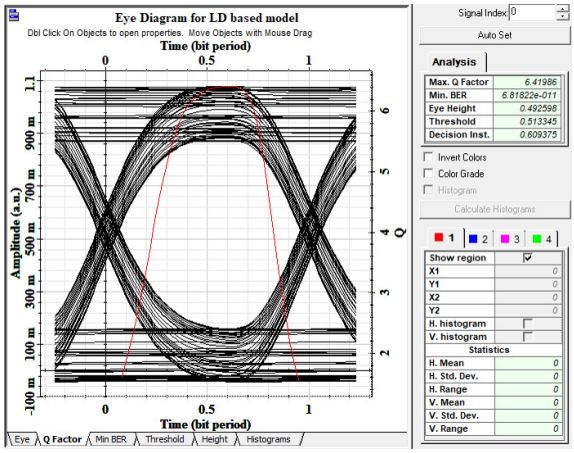

Fig. 17. Eye diagram of the LOS model using LD for a 190 m link distance at 25 Gbps.

The power calculations for the LOS model using LD and without the use of TIA for a 190 m link distance and a 25 Gbps data rate are shown in Table 10. Table 11 shows the obtained power when using TIA in the proposed model.

Table 10.
Obtained power for the proposed LD-based model without the use of TIA.

	Signal power		Noise power	
	Watt	dBm	Watt	dBm
The output power of high beam headlamp	1.393	31.44	0	−100
The output power of channel	$787.5 \cdot 10^{-6}$	−1.03	0	−100
The output power of APD	$205.4 \cdot 10^{-6}$	−6.87	$6.69 \cdot 10^{-3}$	8.257
The output power of LPF	$188.8 \cdot 10^{-6}$	−7.23	$159.2 \cdot 10^{-6}$	−7.98

Table 11.
Power calculations for LOS model using LD and APD.

	Signal power		Noise power	
	Watt	dBm	Watt	dBm
The output power of LD high beam headlamp	1.4	30	0	−100
The output power of the channel	$787 \cdot 10^{-6}$	−1	0	−100
The output power of APD	$205.4 \cdot 10^{-6}$	−6.8	$6.69 \cdot 10^{-3}$	8.257
The output power of TIA	$513.5 \cdot 10^{-3}$	27	$7.16 \cdot 10^{-3}$	8.552
The output power of LPF	$472.1 \cdot 10^{-3}$	26	$7.08 \cdot 10^{3}$	8.5

3.1. Effect of link distance for the second proposed system model.

In this part, the effect of link distance on the maximum Q-factor, BER, and output electrical power is investigated and the results are displayed in Fig. 18 under different weather conditions at a 25 Gbps data rate.

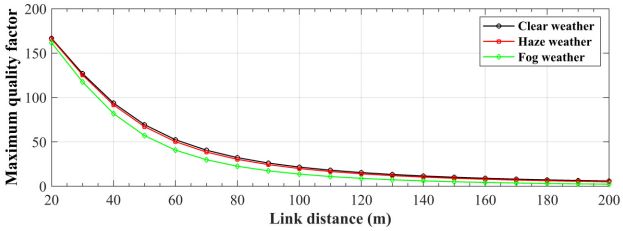

Fig. 18. Maximum Q-factor *vs.* link distance for the LD-based system at 25 Gbps under different weather conditions.

Here, the maximum Q-factor decreases with the link distance. For clear sky, where $\alpha = 0.4$ dB/km, this system can support a link up to 190 m with an acceptable value of the maximum Q-factor of 6.419. For haze weather, where $\alpha = 4$ dB/km, this system can support a link up to 180 m, while for fog weather, where $\alpha = 21$ dB/km, the system can support a link up to 140 m. Thus, the LD-based VVLC system provides a longer link distance and a higher data rate, resulting in a better performance as compared to the LED-based VVLC system.

A comparison between the maximum achievable link distance and the corresponding maximum quality factor for both the LED-based and LD-based models for different weather conditions is shown in Table 12.

Table 12.
Maximum achievable link distance and the corresponding maximum Q-factor for LED-based and LD-based models.

	Max. achievable link distance (m)			Corresponding max. Q-factor		
	Clear	Haze	Fog	Clear	Haze	Fog
LED-based model	80	70	60	6.24	6.98	7.24
LD-based model	190	180	140	6.41	6.15	6.01

The effect of link distance on the BER is shown in Figs. 19–21. The BER increases as the link distance is increased. For a better system performance, the link distance should not exceed 200 m for clear sky weather. At this link distance, the BER is $3 \cdot 10^{-9}$. For haze weather, the link distance should not be higher than 180 m, where the BER is $3.7 \cdot 10^{-10}$. For the worst case of fog weather, the maximum acceptable link distance is 140 m and the BER at this distance is $9.13 \cdot 10^{-10}$.

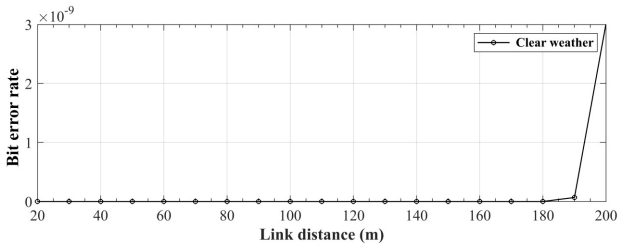

Fig. 19. BER *vs.* link distance for LD-based system at 25 Gbps for clear sky weather.

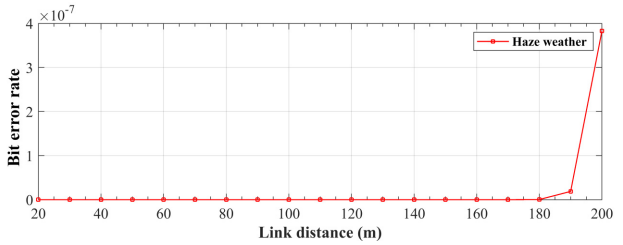

Fig. 20. BER *vs.* link distance for the LD-based system at 25 Gbps, for haze weather.

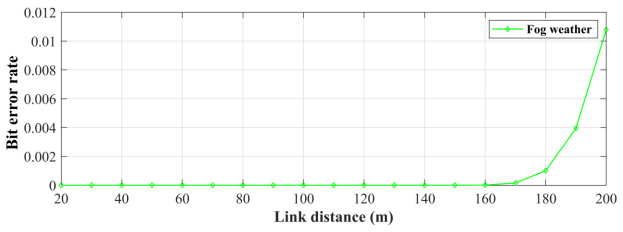

Fig. 21. BER *vs.* link distance for the LD-based system at 25 Gbps, for fog weather.

Table 13 illustrates a comparison between the maximum achievable link distance and the minimum obtained BER for the two proposed models.

Figure 22 illustrates the relation between the output electrical power and the link distance at a data rate of 25 Gbps. Here, the link distance has a strong effect on the output electrical power and also the weather conditions have a great impact on the values of the output power. Compared to the output power obtained from the first proposed model, it is clear that this model is better than the first one (the LED-based one) as there is a great enhancement in the values of the output power even in the worst case of weather conditions.

Table 13.
Maximum achievable link distance and the minimum BER for LED-based and LD-based models.

	Max. achievable link distance (m)			Minimum BER		
	Clear	Haze	Fog	Clear	Haze	Fog
LED-based model	80	80	70	$2 \cdot 10^{-10}$	$9 \cdot 10^{-10}$	$9 \cdot 10^{-10}$
LD-based model	190	180	140	$6 \cdot 10^{-11}$	$3 \cdot 10^{-10}$	$9 \cdot 10^{-10}$

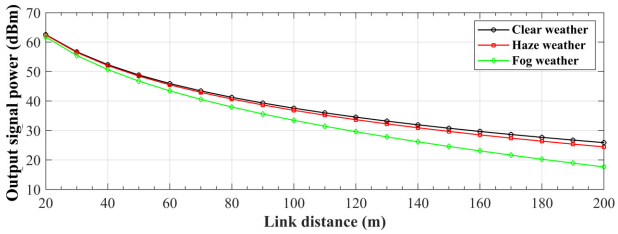

Fig. 22. Output electrical signal power *vs.* link distance for the LD-based system at 25 Gbps.

Table 14 illustrates the comparison between the two proposed models according to the maximum achievable link distance and the output electrical power.

Table 14.
Maximum achievable link distance and the corresponding output electrical power for LED-based and LD-based models.

	Max. achievable link distance (m)			Corresponding output power (dBm)		
	Clear	Haze	Fog	Clear	Haze	Fog
LED-based model	80	70	60	−10	−8.26	−7.59
LD-based model	190	180	140	26.73	26.36	26.15

3.2. *Effect of beam divergence on the performance of the laser diode-based model.*

The beam divergence has a strong effect on the performance of the VVLC system. Figure 23 illustrates the relation between beam divergence and maximum Q-factor for a 140 m link distance and a data rate of 25 Gbps. Clearly, the system provides a good performance at small values of beam divergence. For beam divergence higher than 2 mrad, the value of the maximum Q-factor decreases

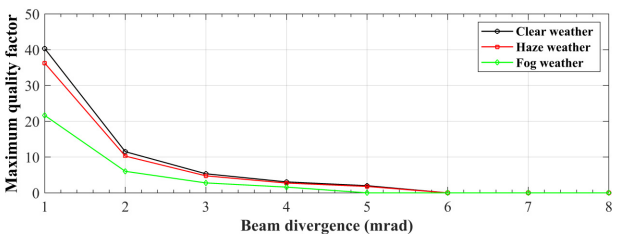

Fig. 23. Maximum Q-factor *vs.* beam divergence for a 140 m link distance at 25 Gbps.

obviously until reaching zero at 5 mrad under fog weather condition.

The relation between beam divergence and the output electrical power is displayed in Fig. 24. The output electrical power decreases with the beam divergence. Also, the output power, in case of fog, has higher deviation than that obtained in the case of both clear and haze weather conditions. At a beam divergence of 2 mrad, the obtained output power for clear, haze, and fog is 31.92, 30.9, and 26.15 dBm, respectively.

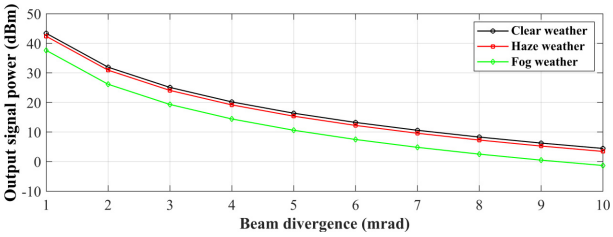

Fig. 24. Output electrical power *vs*. beam divergence for a 140 m link distance at 25 Gbps.

Table 15 shows the maximum suitable beam divergence and the corresponding maximum Q-factor for both proposed models.

Table 15.
Maximum acceptable Q-actor *vs*. beam divergence for both LED and LD based models.

	Max. beam divergence (mrad)			Corresponding max. achievable Q-factor		
	Clear	Haze	Fog	Clear	Haze	Fog
LED-based model	70	68	58	6.03	6	6
LD-based model	2	2	2	11.5	10.27	6.01

3.3. *Effect of transmitter aperture diameter on the performance of the laser-diode-based model.*

The effect of the transmitter aperture diameter on the maximum Q-factor and the output power is being investigated in Fig. 25, showing a significant effect of the transmitter aperture diameter on the maximum Q-factor for clear, hazy, and foggy weather conditions. For good system performance, the transmitter aperture diameter should not exceed 1 cm under the foggy weather condition. Figure 26 shows the effect of the transmitter aperture diameter on the output electrical power, where the output power decreases with the increase in the transmitter aperture diameter. The amount of transmitted power in the case of fog is the lowest compared with that in both clear and hazy weather conditions.

3.4. *Effect of receiver parameters on the performance of the laser-diode-based model.*

In this section, two parameters of the receiver are discussed: responsivity and aperture diameter. Figure 27 displays the effect of the receiver responsivity on the maximum Q-factor. As seen, it is better to choose a suitable type of APD with a receiver responsivity higher than 0.2 A/W. At values smaller than 0.2 A/W, the quality of the system reduces significantly, especially in the case of a foggy weather condition.

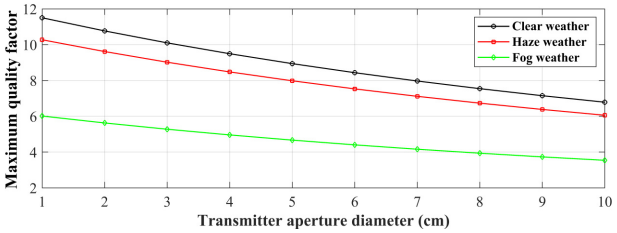

Fig. 25. Maximum Q-factor *vs*. transmitter aperture diameter for a 140 m link distance at 25 Gbps.

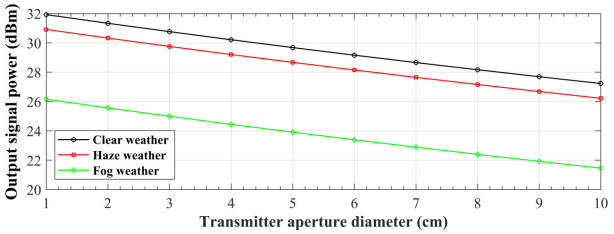

Fig. 26. Output power *vs*. transmitter aperture diameter for a 140 m link distance at 25 Gbps.

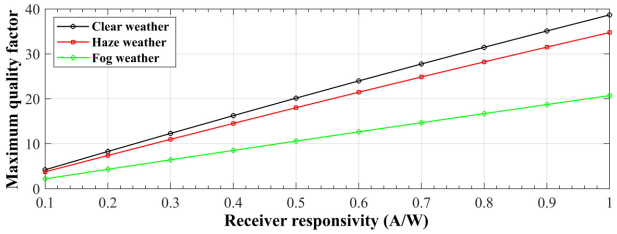

Fig. 27. Maximum Q-factor *vs*. receiver responsivity for a 140 m link distance at 25 Gbps

Table 16 displays the minimum value of the receiver responsivity for achieving the minimum acceptable Q-factor for the LED-based and the LD-based models. Figure 28 illustrates the relation between the maximum Q-factor and receiver aperture diameter for a 140 m link distance at 25 Gbps. It proves that the maximum Q-factor increases significantly as the receiver aperture diameter is increased. Thus, it is better to choose a receiver aperture diameter with a value higher than 1 cm for better system performance.

Table 16.
Minimum Q-factor *vs*. the minimum receiver responsivity for both LED and LD based models.

	Min. receiver responsivity (A/W)			Corresponding min. acceptable Q-factor		
	Clear	Haze	Fog	Clear	Haze	Fog
LED-based model	0.3	0.3	0.4	6.5	6.25	6.16
LD-based model	0.2	0.2	0.3	8.28	7.39	6.43

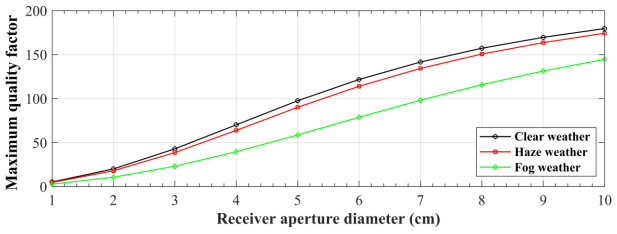

Fig. 28. Maximum Q-factor *vs*. receiver aperture diameter for a140 m link distance at25 Gbps

Table 17 illustrates the minimum value for the receiver aperture diameter for achieving the minimum acceptable Q-factor for both proposed models.

Table 17.
Minimum acceptable Q-actor *vs*. minimum receiver aperture diameter for both LED and LD based models.

	Min. receiver aperture diameter (cm)			Corresponding min. acceptable Q-factor		
	Clear	Haze	Fog	Clear	Haze	Fog
LED-based model	2	2	2	8.12	7.93	6.95
LD-based model	2	2	2	20.06	17.94	10.55

When comparing the previous research work with the two proposed models, it was obvious that the proposed model can achieve higher data rate with a larger link distance when using the LD-based model. The LED-based model provides a longer link distance compared with the previous work. Although the previous research work achieved higher data rates than the proposed LED-based model but these works have neglected the effect of weather conditions and different system parameters on the performance of the system. Table 18 shows a table of comparison between the published previous work and the proposed work.

4. Comparison between mathematical results and simulation results for the two proposed models

Comparisons between the obtained simulation results and the mathematical results for the BER (which was derived in section 2) are illustrated in Tables 19 and 20 for the LED-based model and LD-based model, respectively. For example, for the LED-based model, in the clear weather with a link distance of 80 m and a Q-factor of 6.24, the obtained BER from the simulation result and the eye diagram was $2 \cdot 10^{-10}$ as illustrated in Fig. 4. When calculating the BER using the mathematical equation derived (29), the following result is obtained

$$\text{BER} = 0.5 \operatorname{erfc}\left(\frac{6.24}{\sqrt{2}}\right) = 0.5 \operatorname{erfc}(4.412) \approx 2.18 \cdot 10^{-10}$$

which is approximately the same as that obtained from the simulation, showing an excellent agreement.

Figures 29, 30, and 31 show a comparison between the simulation results and the mathematical results for different weather conditions for the LED-based model, showing a fair agreement.

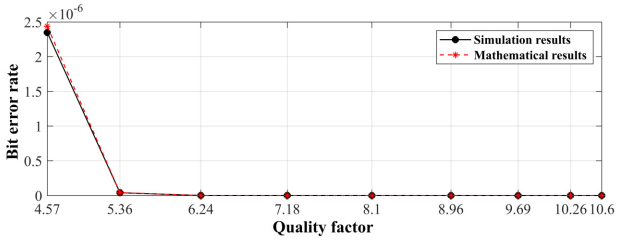

Fig. 29. BER *vs*. Q-factor for clear weather for LED-based model for both simulation results and mathematical results.

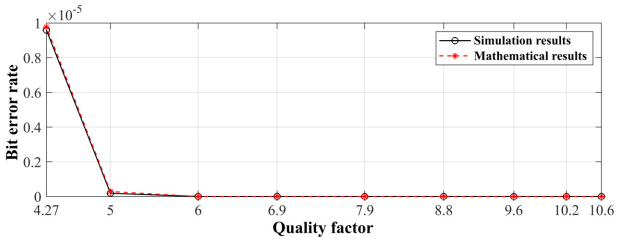

Fig. 30. BER *vs*. Q-actor for haze weather for LED-based model for both simulation results and mathematical results.

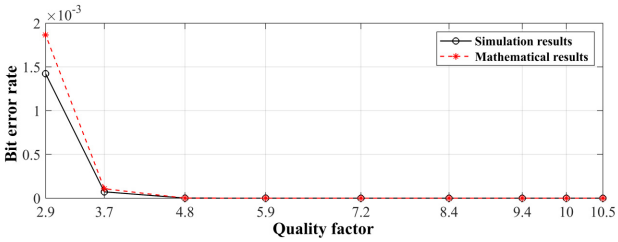

Fig. 31. BER *vs*. Q-factor for fog weather for LED-based model for both simulation results and mathematical results.

Table 18.
Comparison between previous work and proposed work.

Ref.	Optical Tx	Optical Rx	Modulation	Data rate (bps)	Link distance (m)
[6]	LED	PIN	RZ-OOK	20 K	20
[7]	White LED	PIN	NRZ-OOK	2 G	3
[8]	LED	APD	–	100 M and 14 M	2 and 15
[9]	White LED	PIN	OFDM	10 G	2
[10]	LD	PIN	DS-OCDMA	–	100
Proposed work using LED	White LED	APD	NRZ-OOK	60 K	80
Proposed work using LD	LD	APD	NRZ-OOK	25 G	190

Table 19.
Comparison between simulation results and mathematical results for the LED-based model.

	Max. achievable link distance (m)	Obtained Q-factor (Q)	Obtained BER	
			Simulation results	Mathematical results
Clear	80	6.24	$2 \cdot 10^{-10}$	$2.18 \cdot 10^{-10}$
Haze	70	6.9	$1.34 \cdot 10^{-12}$	$1.5 \cdot 10^{-12}$
Fog	60	7.24	$2 \cdot 10^{-13}$	$2.4 \cdot 10^{-13}$

Table 20.
Comparison between simulation results and mathematical results for the LD-based model.

	Max. achievable link distance (m)	Obtained Q-factor (Q)	Obtained BER	
			Simulation results	Mathematical results
Clear	190	6.41	$6 \cdot 10^{-11}$	$7 \cdot 10^{-11}$
Haze	180	6.15	$3 \cdot 10^{-10}$	$3.8 \cdot 10^{-10}$
Fog	140	6.01	$9 \cdot 10^{-10}$	$9.27 \cdot 10^{-10}$

Comparisons between the simulation results and mathematical results for LD-based model for clear, haze, and fog weather conditions are illustrated in Figs. 32, 33, and 34, showing also a fair agreement.

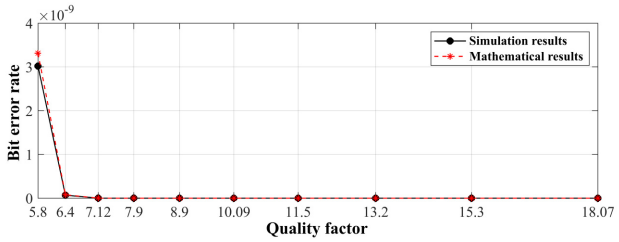

Fig. 32. BER vs. Q-factor for clear weather for LD-based model for both simulation results and mathematical results.

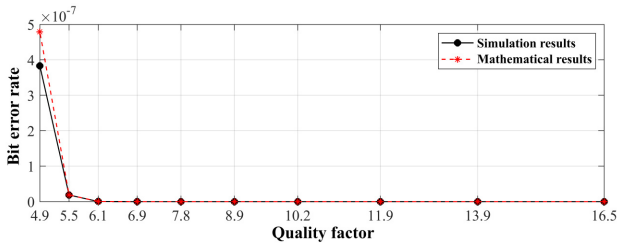

Fig. 33. BER vs. Q-factor for haze weather for LD-based model for both simulation results and mathematical results.

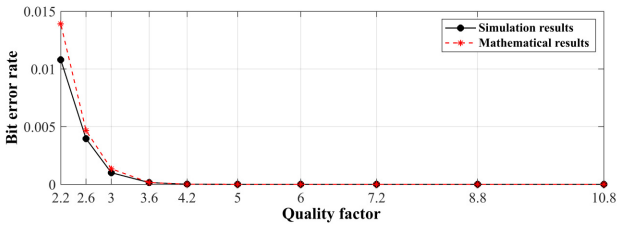

Fig. 34. BER vs. Q-factor for fog weather for LD-based model for both simulation results and mathematical results.

5. Conclusions

Two VVLC system models have been proposed. The first model is a LED-based VVLC system, and the second model is a LD-based VVLC system. Performance evaluation for both systems is performed through the Q-factor, BER, and output power. A TIA can be used to enhance the output power at the receiving end for both models. The obtained results show that in the presence of the TIA, the output power of the LED-based and LD-based VVLC systems increased by 98.46 μW and 0.4719 W, respectively. On the other hand, the maximum achievable link distance for the LD-based and LED-based VVLC systems is 190 m with a data rate of 25 Gbps and 80 m with a data rate of 60 kbps, respectively, with the same system parameters and weather conditions. In comparison to the LED-based VVLC system, which can support links up to 80 m, 70 m, and 60 m with an acceptable BER of $2.02 \cdot 10^{-10}$, $9.62 \cdot 10^{-10}$, and $9.93 \cdot 10^{-10}$ for a data rate of 60 kbps for clear, haze, and fog weather conditions, respectively, the LD-based VVLC system can support links up to 190 m, 180 m, and 140 m with a minimum acceptable BER of $3 \cdot 10^{-9}$, $3.7 \cdot 10^{-10}$, and $9.13 \cdot 10^{-10}$ for a data rate of 25 Gbps for the three different weather conditions. In addition, the LD-based VVLC system produces higher values for the maximum Q-factor than the LED-based VVLC-LED system. With regards to the output power, in the foggy weather, the lowest output power for the LD-based VVLC system is 17.623 dBm at a link distance of 200 m, as opposed to −4.06 dBm for the LED-based VVLC system at a link distance of 50 m. Therefore, the LD-based VVLC system has an additional benefit over the LED-based VVLC system having higher output power.

On the other hand, different system parameters also affect the system performance significantly, such as beam divergence, receiver aperture diameter, receiver responsivity, and quantum efficiency. The beam divergence affects the performance of both models significantly. The beam divergence affects the performance of both models significantly, as well. The minimum acceptable value of the maximum Q-factor obtained was 6 at 58 mrad and 6.01 at 2 mrad, for LED-based and LD-based VVLC systems, respectively. This value was considered for fog weather. From the point of view of the receiver aperture diameter, the LD-based VVLC system shows better performance than that of the LED-based one, where the LD-based VVLC achieves a Q-factor of 2.7 to 144.54 for a receiver aperture diameter of 1 to 10 cm, while the corresponding values of the LED-based VVLC system are 2.3 to 10.68. The APD receiver responsivity also shows better performance in the LD-based VVLC with 0.3 A/W, compared to 0.4 A/W for the LED-based one. Therefore, with the proper selection of the system parameters, the performance of the system can be enhanced. The obtained results reveal that the performance of the LD-based VVLC system outperforms the LED-based one. The results also ensure the relevance of the proposed system for automotive applications under different weather conditions, such as clear, hazy, and foggy weather. It is also concluded that the obtained simulation results for the BER are approximately the same as that obtained from the mathematical analysis, showing an excellent agreement.

In the future, the performance of LD-based VVLC system could be investigated in the case of the NLOS model by adding the effect of external light sources and finding new approaches for enhancing the system performance by limiting the effect of external light sources.

References.

[1] El-Mokadem, E. S., El-Kassas, A. M., Elgarf, T. A. & El-Hennawy, H. BER performance Evaluation For The Downlink NOMA System Over Different Fading Channels With Different Modulation Schemes. in *5th IEEE International Conference on Science and Technology (ICST)* 1–6 (2019). https://doi.org/10.1109/ICST47872.2019.9166288

[2] El-Mokadem, E. S., El-Kassas, A. M., Elgarf, T. A. & El-Hennawy, H. Throughput enhancement of cognitive M2M networks based on NOMA for 5G communication systems. *Int. J. Commun. Syst.* **33**, e4468 (2020). https://doi.org/10.1002/dac.4468

[3] Yahia, S. *et al.* Performance study and analysis of MIMO visible light communication-based V2V systems. *Opt. Quantum Electron.* **54**, 1–22 (2022). https://doi.org/10.1007/s11082-022-04015-w

[4] Zhang, J. & Huang, S. Improving the performance of uplink visible light communication in urban streets. *J. Supercomput.* **78**, 3775–3790 (2022). https://doi.org/10.1007/s11227-021-04010-0

[5] Faheem, M., Verma, I. K., Nag, P., Goswami, S. & Singh, V. Performance Analysis of Indoor Visible Light Communication System Using NRZ-OOK Modulation Technique. in *Advances in Smart Communication and Imaging Systems* (eds. Agrawal, R., Kishore Singh, C. & Goyal, A.) 453–466 (Springer, 2021). https://doi.org/10.1007/978-981-15-9938-5_43

[6] Sindhubala, K. & Vijayalakshmi, B. Simulation of VLC system under the influence of optical background noise using filtering technique. *Materials Today: Proc.* **4**, 4239–4250 (2017). https://doi.org/10.1016/j.matpr.2017.02.127

[7] Manivannan, K., Raja, A. S. & Selvendran, S. Performance investigation of visible light communication system using optisystem simulation tool. *Int. J. Microw. Opt. Technol.* **11**, 377–383 (2016).

[8] Béchadergue, B. *et al*. Vehicle-to-Vehicle Optical Wireless Communication With The Smart Corner ™ Automotive Headlamp. in *Global LIFI Congress (GLC)* 1–5 (IEEE, 2019) https://hal.science/hal-02398747/document

[9] Selvendran, S., Sivanantha Raja, A., Esakki Muthu, K. & Lakshmi, A. Certain investigation on visible light communication with OFDM modulated white LED using optisystem simulation. *Wirel. Pers. Commun.* **109**, 1377–1394 (2019). https://doi.org/10.1007/s11277-019-06617-2

[10] Kharbouche, A., Madini, Z. & Zouine, Y. Analysis of Realistic DS-OCDMA/VLC for V2X Communication Using Optisystem. in *7th International Conference on Optimization and Applications (ICOA)* 1–5 (IEEE, 2021). https://doi.org/10.1109/ICOA51614.2021.9442666

[11] Siegel, T. & Chen, S.-P. Investigations of free space optical communications under real-world atmospheric conditions. *Wirel. Pers. Commun.* **116**, 475–490 (2021). https://doi.org/10.1007/s11277-020-07724-1

[12] Brima, A. B. S., Ataro, E. & Kamagate, A. Performance enhancement of an FSO link using polarized quasi-diffuse transmitter. *Heliyon* **7**, e08248 (2021). https://doi.org/10.1016/j.heliyon.2021.e08248

[13] Karbalayghareh, M. *et al.* Channel modelling and performance limits of vehicular visible light communication systems. *IEEE Trans. Veh. Technol.* **69**, 6891–6901 (2020). https://doi.org/10.1109/TVT.2020.2993294

[14] Ndjiongue, A. R. & Ferreira, H. C. An overview of outdoor visible light communications. *Trans. Emerg. Telecommun. Technol.* **29**, e3448 (2018). https://doi.org/10.1002/ett.3448

[15] Padhy, J. B. & Patnaik, B. Link performance evaluation of terrestrial FSO model for predictive deployment in Bhubaneswar smart city under various weather conditions of tropical climate. *Opt. Quantum Electron.* **53**, 1–24 (2021). https://doi.org/10.1007/s11082-020-02702-0

[16] Idris, S., Aibinu, A. M., Koyunlu, G. & Sanusi, J. A Survey of Modulation Schemes in Visible Light Communications. in *3rd International Conference on Trends in Electronics and Informatics (ICOEI)* 1–7 (IEEE, 2019) https://doi.org/10.1109/ICOEI.2019.8862538

[17] Lorences-Riesgo, A. *et al.* 200 G outdoor free-space-optics link using a single-photodiode receiver. *J. Light. Technol.* **38**, 394–400 (2020). https://doi.org/10.1109/ICOEI.2019.8862538

[18] Schirripa Spagnolo, G., Cozzella, L. & Leccese, F. Underwater optical wireless communications: Overview. *Sensors* **20**, 2261 (2020). https://doi.org/10.3390/s20082261

[19] Farahneh, H., Hussain, F. & Fernando, X. Performance analysis of adaptive OFDM modulation scheme in VLC vehicular communication network in realistic noise environment. *EURASIP J. Wirel. Commun. Netw.* **2018**, 1–15 (2018). https://doi.org/10.1186/s13638-018-1258-3

[20] Yanikgonul, S. *et al.* Integrated avalanche photodetectors for visible light. *Nat. Commun.* **12**, 1834 (2021). https://doi.org/10.1038/s41467-021-22046-x

[21] Torres-Zapata, E., Guerra, V., Rabadan, J., Luna-Rivera, M. & Perez-Jimenez, R. VLC network design for high mobility users in urban tunnels. *Sensors* **22**, 88 (2021). https://doi.org/10.3390/s22010088

[22] Fernando, X. & Farahneh, H. *Visible Light Communications: Vehicular Applications* (IOP Publishing: Bristol, 2019).

[23] Eldeeb, H. B., Elamassie, M., Sait, S. M. & Uysal, M. Infrastructure-to-Vehicle visible light communications: channel modelling and performance analysis. *IEEE Trans. Veh. Technol.* **71**, 2240–2250 (2022). https://doi.org/10.1109/TVT.2022.3142991

[24] El-Nayal, M. K., Aly, M. M., Fayed, H. A. & AbdelRassoul, R. A. Adaptive free space optic system based on visibility detector to overcome atmospheric attenuation. *Results Phys.* **14**, 102392 (2019). https://doi.org/10.1016/j.rinp.2019.102392

[25] Georlette, V. *et al.* Outdoor visible light communication channel modeling under smoke conditions and analogy with fog conditions. *Optics* **1**, 259–281 (2020). http://doi.org/10.3390/opt1030020

[26] Ghassemlooy, Z., Popoola, W. & Rajbhandari, S. *Optical wireless communications: system and channel modelling with Matlab®, 2nd edition*. (CRC Press, Boca Raton, 2019). https://doi.org/10.1201/9781315151724